

Frequency Dependent Invasion in a Spatial Environment

Frank Schweitzer,^{1,2,*} Laxmidhar Behera,^{1,3} and Heinz Mühlenbein¹

¹Fraunhofer Institute for Autonomous Intelligent Systems,
Schloss Birlinghoven, 53754 Sankt Augustin, Germany

²Institute of Physics, Humboldt University, Newtonstraße 15, 12489 Berlin, Germany

³Department of Electrical Engineering, Indian Institute of Technology, Kanpur 208 016, India

(Dated: July 23, 2003)

We investigate the spatio-temporal dynamics of two species in a two-dimensional system. The spread of each species depends non-linearly on the local frequency of its kind in its surrounding (expressed by two parameters α_1, α_2), which allows us to consider both positive and negative frequency dependence. For different α_1, α_2 , computer simulations on a cellular automaton show either formation of spatial domains that grow until complete invasion of one species is reached, or coexistence of both species, which could occur in random or non-stationary spatial patterns. Based on the microscopic dynamics, equations for macroscopic key variables are derived and investigated analytically by means of mean-field and pair approximations. We show that the latter is in good agreement with observed global frequency and spatial correlations. Furthermore, the pair approximation allows us to derive a phase diagram in the (α_1, α_2) space, from which we are able to distinguish between the three different spatial-temporal regimes observed, in agreement with the CA simulations.

PACS numbers: 87.23.Cc, 87.23.Ge

I. INTRODUCTION

In biological systems, the survival of a species depends on the frequencies of its kin and its foes in the environment [1, 2]. In some cases, the chance of survival of a certain species *improves* as the frequency of its kind increases, since this might enhance the chance for reproduction or other benefits from group interaction. This is denoted as *positive* frequency dependence. In other cases a *negative* frequency dependence, that is the increase of the survival chance with *decreasing* frequency, is observed. This is the case, when individuals compete for rare resources. Moreover, negative frequency dependence is known to be important for maintaining the genetic diversity in natural populations [3, 4].

Frequency dependent dynamics are not only found in biological systems, but also in social and economic systems [5, 6, 7, 8, 9, 10, 11]. In democracies, a simple example is a public vote, where the winning chances of a party increase with the number of supporters [12, 13]. In economics, e.g. the acceptance of a new products may increase with the number of its users [14]. In stock markets, on the other hand, positive and negative frequency dependencies may interfere. For instance, the desire to buy a certain stock may increase with the orders observed from others, a phenomenon known as the *herding effect*, but it also may decrease, because traders fear speculative bubbles.

In general, many biological and socio-economic processes are governed by the frequency dependent adoption of a certain behavior or strategy, or simply by fre-

quency dependent reproduction. In order to model such dynamics more rigorously (but less concrete), different versions of *non-linear voter models* have been investigated. Here, the transition rate $w(\theta|\theta')$ from state θ' to state θ (where *state* could stand for opinion, attitude, or occupation etc.) is assumed to be a function of the frequency f_θ , $w(\theta|\theta') = \kappa(f) f_\theta$. The non-linearity is expressed in terms of the (frequency dependent) prefactor κ . Linear voter models have been discussed for a long time in mathematics [15, 16, 17, 18], while non-linear voter models have been of particular interest to population biologists [2].

Depending on how the frequency f_θ is estimated, one can further distinguish between global and local voter models. In the latter case the transition is governed only by the local frequency of a certain state in a given neighborhood. In contrast to global (or mean-field) models, this will lead to spatial effects in the dynamics, which are also of particular interest in the current paper. If space is represented by a two-dimensional lattice and each site is occupied by just one individual, then each species occupies an amount of space proportional to its presence in the total population. Local effects such as the occupation of a neighborhood by a particular species or the adoption of a given opinion in a certain surrounding, can then be observed graphically in terms of domain formation. This way, the invasion of species (or opinions) in the environment displays obvious analogies to spatial pattern formation in physical systems.

Physicists have developed different spatial models for such processes. One recent example is the so-called “Sznajd model” [19, 20, 21] which is a simple cellular automata approach to consensus formation (i.e. complete invasion) among two opposite opinions (described by spin up or down). In [22], we have shown that the Sznajd model can be completely reformulated in terms of a lin-

*corresponding author; schweitzer@ais.fraunhofer.de;
<http://www.ais.fraunhofer.de/~frank/>

ear voter model, where the transition rates towards a given opinion are directly proportional to the frequency of the respective opinion of the *second-nearest* neighbors and independent of the nearest neighbors.

Other spatial models are proposed for game-theoretical interactions among nearest neighbors [23, 24, 25]. Here, the dynamics are driven by local payoff differences of adjacent players, which basically determine the non-linearity $\kappa(f)$. Depending on these payoff differences, we could derive a phase diagram with five regimes, each characterized by a distinct spatio-temporal dynamic [26]. The corresponding spatial patterns range from complete invasion to coexistence with large domains, coexistence with small clusters, and spatial chaos.

In this paper, we are interested in the spatial effects of frequency dependent dynamics, where the non-linearity $\kappa(f)$ can be simply expressed by two constants, α_1, α_2 . This is a special form of a non-linear voter model, which for $\alpha_1 < \alpha_2 < 0.5$ also includes majority voting and for $\alpha_1 > \alpha_2 > 0.5$ minority voting. We investigate the spatio-temporal dynamics of this model both analytically and by means of computer simulations on a two-dimensional stochastic cellular automaton. In Sect. II, we introduce the microscopic model of frequency dependent invasion and demonstrate the role of α_1, α_2 by means of characteristic pattern formation. Based on the microscopic description, in Sect. III we derive the dynamics for the global frequency $x(t)$, which is a macroscopic key variable. An analytical investigation of these dynamics is made possible by pair approximation, which results in a closed-form description for $x(t)$ and the spatial correlations $c_{11}(t)$. In Sect. IV, we verify the performance of our analytical approximations by comparing them with averaged CA computer simulations. The outcome of the comparison allows us to derive, in Sect. V, a phase diagram in the (α_1, α_2) parameter space, to distinguish between two possible dynamic scenarios: (i) complete invasion of one of the species, with formation of domains at intermediate time scales, and (ii) random spatial coexistence of two species. A third dynamic regime, the non-stationary coexistence of the two species on long time scales together with the formation of spatial domains, can be found in a small, but extended region that separates the two dynamic regimes mentioned above. We further show that the usual distinctions for the dynamics, such as positive or negative frequency dependence, do not necessarily coincide with the different dynamic regimes. Instead, for positive frequency dependence, all of the three different dynamic regimes (and the related spatio-temporal patterns) are observed. In the Appendix, calculation details for the pair approximation are given.

II. MICROSCOPIC MODEL OF INVASION

A. Defining the cellular automaton

We consider a model of two species labeled by the index $\sigma = \{0, 1\}$. The total number of individuals is constant, so the global frequency x_σ (or the share of each species in the total population) is defined as:

$$N = \sum_{\sigma} N_{\sigma} = N_0 + N_1 = \text{const.}$$

$$x_{\sigma} = \frac{N_{\sigma}}{N}; \quad x \equiv x_1 = 1 - x_0 \quad (1)$$

In the following, the variable x shall refer to the global frequency of species 1.

The individuals of the two species are assumed to be spatially distributed on a regular two-dimensional lattice. Therefore, we consider a two-dimensional cellular automaton (CA) consisting of N cells, that can be numbered consecutively. Each cell is identified by the index $i \in N$ that also refers to its spatial position. We note that in most two-dimensional CA the position of the cells are identified by ij coordinates referring to the two dimensions. However, in order to define neighborhoods and to simplify the notations, we will use only index i for the spatial position. This implies that the description derived in the following may also apply to one-dimensional CA provided the neighborhoods are defined accordingly [27].

Each cell is occupied by one individual, and thus characterized by a discrete value $\theta_i \in \{0, 1\}$ indicating whether it is occupied by an individual of species 0 or 1. The spatio-temporal distribution of the individuals is then described by

$$\Theta = \{\theta_1, \theta_2, \dots, \theta_N\} \quad (2)$$

Note that the state space Ω of all possible configurations is of the order 2^N .

In the spatial model of frequency dependent invasion, the dynamic of Θ is governed by the *occupation distribution* of the *local neighborhood* that surrounds each cell i . If we define the size of a neighborhood by n (including cell i), the different neighbors of i are characterized by a second index $j = 1, \dots, n-1$. The numbering starts with the nearest neighbors (cf. Fig. 1). Note that $\theta_i \equiv \theta_{i_0}$ (i.e. $j=0$).

In this paper, local effects shall be restricted only to the m nearest neighbors of cell i , i.e. $n = m + 1$. For further use, we define the local occupation $\underline{\theta}_i$ of the nearest neighborhood (without cell i) as:

$$\underline{\theta}_i = \{\theta_{i_1}, \theta_{i_2}, \dots, \theta_{i_m}\} \quad (3)$$

A specific realization of this distribution shall be denoted as $\underline{\sigma}$, while the function $\underline{\eta}_i(\underline{\sigma})$ assigns $\underline{\sigma}$ to a particular neighborhood $\underline{\theta}_i$:

$$\underline{\sigma} = \{\sigma_1, \sigma_2, \dots, \sigma_m\}$$

$$\underline{\eta}_i(\underline{\sigma}) = \{\theta_{i_1} = \sigma_1, \theta_{i_2} = \sigma_2, \dots, \theta_{i_m} = \sigma_m\} \quad (4)$$

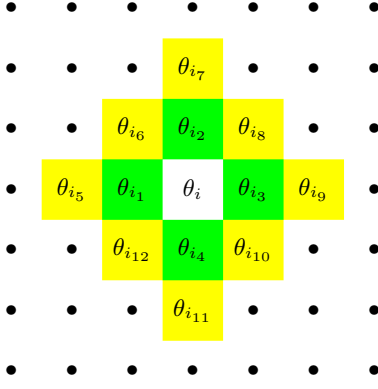


FIG. 1: Sketch of the two-dimensional cellular automaton. It shows a neighborhood of size n of cell i where the neighbors are labeled by a second index $j = 1, \dots, n-1$. The value $\theta_{i_j} \in \{0, 1\}$ indicates whether the cell is occupied either by an individual of species 0 or 1. The nearest neighbors are shown in darker gray, the second nearest neighbors in lighter gray.

For practical reasons, it is convenient to define these distributions also for the nearest neighborhood *including* cell i :

$$\begin{aligned} \underline{\theta}_i^0 &= \{\theta_i, \theta_{i_1}, \theta_{i_2}, \dots, \theta_{i_m}\} = \underline{\theta}_i \cup \{\theta_i\} \\ \underline{\sigma}^0 &= \{\sigma, \sigma_1, \sigma_2, \dots, \sigma_m\} \\ \eta_i^0(\underline{\sigma}^0) &= \{\theta_i = \sigma, \theta_{i_1} = \sigma_1, \theta_{i_2} = \sigma_2, \dots, \theta_{i_m} = \sigma_m\} \end{aligned} \quad (5)$$

For the given CA with $m=4$, $\underline{\sigma}^0$ denotes a binary string, e.g. $\{01001\}$, where the first value σ refers to the center cell and the other values $\sigma_j \in \{0, 1\}$ indicate the particular values of the nearest neighbors in the order given in Fig. 1. The assignment of these values to a particular neighborhood $\underline{\theta}_i^0$ of cell i is then described by $\eta_i^0(\underline{\sigma}^0)$.

B. Stochastic approach

In a stochastic CA, we consider the probability $p(\Theta, t)$ of finding a particular spatial configuration at time t . If t is measured in discrete time steps (generations) and the CA is synchronously updated, the time-dependent change of $p(\Theta, t)$ is described as follows:

$$p(\Theta, t + \Delta t) = \sum_{\Theta'} p(\Theta, t + \Delta t | \Theta', t) p(\Theta', t) \quad (6)$$

where Θ' denotes all possible realizations of Θ and $p(\Theta, t + \Delta t | \Theta', t)$ denote the conditional probabilities to go from state Θ' at time t to Θ at time $t + \Delta t$. Eq. (6) is based on the Markov assumption that the dynamics at time $t + \Delta t$ may depend only on states at time t . With the assumption of small time steps Δt and the definition

of the transition rates

$$w(\Theta | \Theta', t) = \lim_{\Delta t \rightarrow 0} \frac{p(\Theta, t + \Delta t | \Theta', t)}{\Delta t} \quad (7)$$

eq. (6) can be transferred into a time-continuous master equation as follows:

$$\frac{d}{dt} p(\Theta, t) = \sum_{\Theta'} \left[w(\Theta | \Theta') p(\Theta', t) - w(\Theta' | \Theta) p(\Theta, t) \right] \quad (8)$$

In eq. (8), the transition rates depend on the *whole* distribution Θ . However, in the frequency dependent invasion processes discussed in this paper, only the occupation distribution of the *local* neighborhood of cell i needs to be taken into account. Therefore, it is appropriate to think about some reduced description in terms of lower order distributions, such as the local occupation $\underline{\theta}_i$, eq. (3). In principle, there are two different ways to solve this task. The first one, the *top-down* approach starts from the *global* distribution Θ in the whole state space and then uses different approaches to factorize $p(\Theta, t)$. However, a Markov analysis [28] can only be carried out exactly for small N , because of the exponential N -dependence of the state space. Thus, for larger N suitable approximations, partly derived from theoretical concepts in computer science [29, 30, 31, 32, 33], need to be taken into account.

In this paper, we follow the second approach. Instead of a *mesoscopic* analysis of *probabilities*, $p(\Theta, t)$ we want to derive the dynamics for some appropriate *macroscopic* variables describing the frequency-dependent invasion process. Therefore, we use the *bottom-up* approach, starting with a *local* description that considers only cell i and its local neighborhood. The probability $p_i(\theta_i, t)$ to find cell i in state θ_i depends on the local occupation distribution $\underline{\theta}_i$ of the neighborhood (eq. (3)) in the following manner:

$$p_i(\theta_i, t) = \sum_{\underline{\theta}_i'} p(\theta_i, \underline{\theta}_i', t) \quad (9)$$

Hence, $p_i(\theta_i, t)$ is defined as the marginal distribution of $p(\theta_i, \underline{\theta}_i, t)$, where $\underline{\theta}_i'$ in eq. (9) indicates the summation over all possible realizations of the local occupation distribution $\underline{\theta}_i$, namely 2^{n-1} different possibilities.

For the time dependent change of $p_i(\theta_i, t)$ we assume the following master equation:

$$\begin{aligned} \frac{d}{dt} p_i(\theta_i, t) &= \sum_{\underline{\theta}_i'} \left[w(\theta_i | (1-\theta_i), \underline{\theta}_i') p(1-\theta_i, \underline{\theta}_i', t) \right. \\ &\quad \left. - w(1-\theta_i | \theta_i, \underline{\theta}_i') p(\theta_i, \underline{\theta}_i', t) \right] \quad (10) \end{aligned}$$

where $w(\theta_i | (1-\theta_i), \underline{\theta}_i)$ denotes the transition rate for state $(1-\theta_i)$ of cell i into state θ_i in the next time step under the condition that the local occupation distribution is given by $\underline{\theta}_i$. The transition rate for the reverse process is $w(1-\theta_i | \theta_i, \underline{\theta}_i)$. Again, the summation is over all possible realizations of $\underline{\theta}_i$, denoted by $\underline{\theta}_i'$.

Thus, instead of one equation for $p(\Theta, t)$ in the top-down approach, in the bottom-up approach we now have a set of N stochastic equations for $p_i(\theta_i, t)$, which are locally coupled because of overlapping neighborhoods, $\underline{\theta}_i$. In order to solve the dynamics, we need to discuss suitable approximations for these local correlations. As mentioned earlier, we are interested in the macroscopic dynamics, so these approximations will be done at the macroscopic level. In order to do so, we first derive a macroscopic equation from the stochastic eq. (10), which is carried out in Sect. III A. But before we do that, we have to define the transition rates for the frequency dependent invasion process accordingly.

C. Transition rates for frequency dependent invasion

The basic assumption for the frequency dependent invasion dynamics is that the change of θ_i does not directly depend on the local distribution $\underline{\theta}_i$, but only on the *occupation frequency* of the neighborhood of size n , i.e. on the *number* of cells occupied either by (individuals belonging to the species) 0 or 1. Let us define the *local frequencies* in the neighborhood as:

$$z_i^\sigma = \frac{1}{n} \sum_{j=0}^{n-1} \delta_{\sigma\theta_{i_j}} ; \quad z_i^{(1-\sigma)} = 1 - z_i^\sigma \quad (11)$$

where δ_{xy} is the Kronecker delta, which is 1 only for $x = y$ and zero otherwise. Then, assuming a neighborhood of size $n = m+1 = 5$ (i.e. influence of nearest neighbors only) and $\theta_i = \sigma$, the transition rates defined as follows:

z_i^σ	$z_i^{(1-\sigma)}$	$w(1-\theta_i \theta_i=\sigma, z_i^\sigma)$	
1	0	ε	
4/5	1/5	α_1	(12)
3/5	2/5	α_2	
2/5	3/5	$\alpha_3 = 1 - \alpha_2$	
1/5	4/5	$\alpha_4 = 1 - \alpha_1$	

Eq. (12) means that a particular cell i currently in state $\theta_i = \sigma$, or occupied by an individual of species σ where σ is either 0 or 1, will be occupied by an individual of species $(1-\sigma)$ with a rate $w(1-\theta_i|\theta_i=\sigma, z_i^\sigma)$ that changes with the local frequency z_i^σ in a *non-linear* manner. The general case of four independent transition rates α_i ($i=1, \dots, 4$) in eq. (12) can be reduced to two transition rates α_1, α_2 by assuming a symmetry of the invasion dynamics of the two species, i.e. $\alpha_2 + \alpha_3 = 1$ and $\alpha_1 + \alpha_4 = 1$, which is also satisfied by the assumption of a frequency dependent process. The rate ε in eq. (12) applies for the case where cell i in state σ is surrounded only by individuals of the same kind. In a deterministic model, there would be no need to change the current state. In a stochastic CA however all possible processes should have a certain non-zero probability to occur, wherefore a

rather small value $\varepsilon \approx 0$ is used to avoid dead-locks in the dynamics.

If the transition rates α_1, α_2 are directly proportional to $z^{(1-\sigma)}$, i.e. $\alpha_1 = 0.2$ and $\alpha_2 = 0.4$, this is known as the *linear voter model* that has been investigated mathematically [15, 16, 18]. However, dependent on the relation of the two essential parameters α_1, α_2 *non-linear* voter models can also be considered:

$$\begin{aligned} \text{(pf)} \quad & 0 \leq \alpha_1 \leq \alpha_2 \leq (1 - \alpha_2) \leq (1 - \alpha_1) \leq 1 \\ \text{(nf)} \quad & 1 \geq \alpha_1 \geq \alpha_2 \geq (1 - \alpha_2) \geq (1 - \alpha_1) \geq 0 \\ \text{(pa)} \quad & 0 \leq \alpha_1 \leq \alpha_2, \alpha_2 \geq (1 - \alpha_2), \\ & (1 - \alpha_2) \leq (1 - \alpha_1) \leq 1 \\ \text{(na)} \quad & 1 \geq \alpha_1 \geq \alpha_2, \alpha_2 \leq (1 - \alpha_2), \\ & (1 - \alpha_2) \geq (1 - \alpha_1) \geq 0 \end{aligned} \quad (13)$$

Note, that the parameters $\alpha_1, \dots, \alpha_4$ can be ordered in 24 different ways. These reduce to 8 inequalities under the conditions $\alpha_3 = 1 - \alpha_2$ and $\alpha_4 = 1 - \alpha_1$. In eq. (13), (pf) means (pure) *positive frequency dependent invasion*, where the transition rate *increases* with an increasing number of individuals of the *opposite* species $(1-\sigma)$ in the neighborhood, and (nf) means (pure) *negative frequency dependent invasion* because the transition rate *decreases*. The two other cases describe positive (pa) and negative (na) *allee effects* [2]. These regions are described by 3 inequalities each, all of which show the same relative change in parameter values, if going from α_1 to α_4 . This can be roughly visualized as an up-down-up change in region (pa) and a down-up-down change in region (na). The different parameter regions are shown in Fig. 2. On a first glimpse, one would expect that the spatial dynamics as well as the evolution of global variables may be different in these regions. Thus, one of the aims of this paper is to investigate whether or to what extent this would be the case.

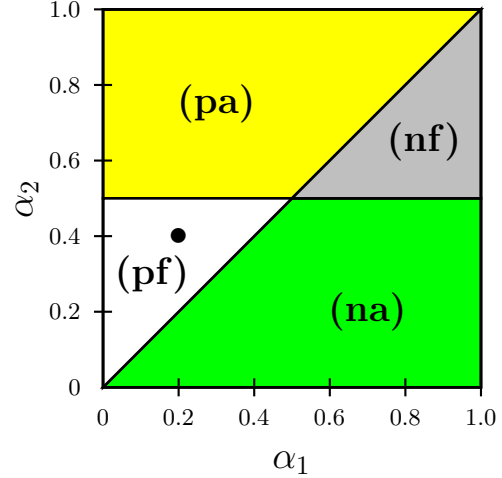


FIG. 2: Four different parameter regions for frequency dependent invasion, according to eq. (13). The linear voter point is indicated by •

D. Computer simulations of the CA model

For a first insight into the dynamics, we have conducted stochastic simulations of the CA described above with different sets of the parameters α_1 , α_2 and ε . In this section, we refer to particular runs and show some snapshots of the spatial dynamics. In Sect. IV averaged simulation results of the global variables are discussed.

In our simulations, we use a CA with periodic boundary conditions and *synchronous update* of the cells. The time scale is defined by the number of simulation steps. If not stated otherwise, the initial configuration of the CA is taken to be a homogeneous distribution (within reasonable limits) of both species, i.e. initially each cell is randomly assigned one of the possible states, $\{0, 1\}$. Then, the initial global frequency is $x(t=0) = 0.5$. We use Monte Carlo simulations, i.e. at each time step, the transition rate is calculated for each cell according to eq. (12) and the values are compared with a random number rnd drawn from the interval $\{0, 1\}$. If rnd is less than the calculated transition rate, the respective transition process is carried out, otherwise the cell remains in its current state. Since each transition only depends on the current local configuration, memory effects are not considered here.

From the description above, it follows that the case $\alpha_1 = 0$, $\alpha_2 = 0$, $\varepsilon = 0$ refers to a *deterministic* positive frequency invasion process, simply because the state of cell i *never* changes as long as at least half of the nearest neighbor cells are occupied by the same species. On the other hand, it will *always* change if more than half of the neighboring cells are occupied by the *other* species. Similarly, a *deterministic* negative frequency invasion process is described by $\alpha_1 = 1$, $\alpha_2 = 1$, $\varepsilon = 0$

Fig. 3 shows spatial snapshots of computer simulations of the deterministic dynamics for both positive and negative frequency dependent invasion. The initial condition is set to $x(t=0) = 0.5$. From the series of snapshots we deduce the following properties of the *deterministic* invasion process:

1. A spatial coexistence of both species is observed in both cases of positive and negative frequency dependence. The global frequency in the stationary state is $x^{\text{stat}} = 0.5$.
2. For the positive frequency dependence the spatial pattern becomes stationary after a short time. For negative frequency dependence the pattern flips between two different configurations with every time step. So, despite a constant global frequency $x^{\text{stat}} = 0.5$, local reconfigurations prevent the pattern from reaching a completely stationary state.
3. In both – positive and negative – frequency dependence cases, individuals of the same species tend to aggregate in space, albeit in different local patterns. For the positive frequency dependence, we

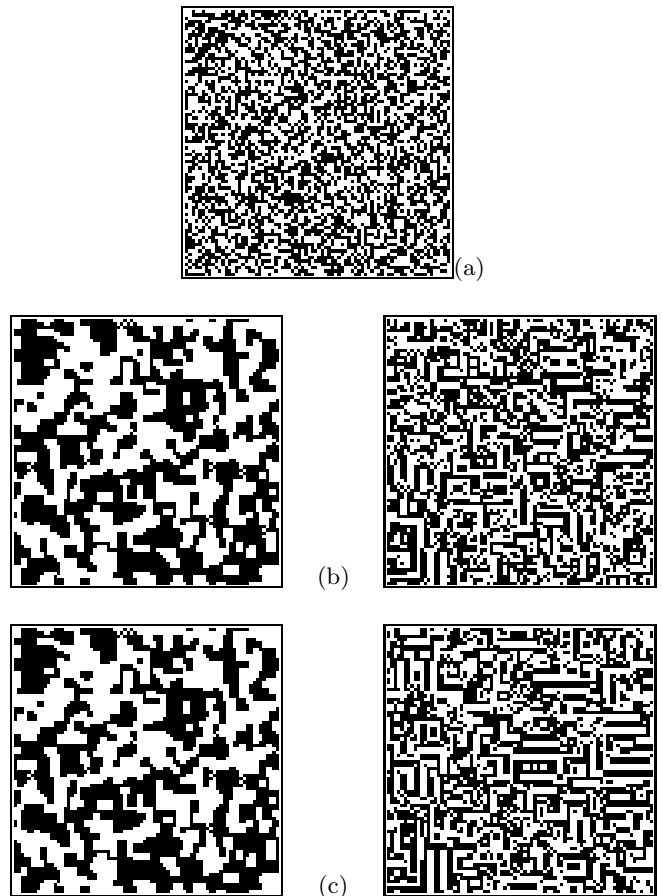


FIG. 3: Spatial snapshots of a deterministic frequency dependent invasion process. (a) $t = 0$ (initial state), (b) $t = 10^1$ (c) $t = 10^2$. The left column refers to positive frequency dependent invasion ($\alpha_1 = 0$, $\alpha_2 = 0$, $\varepsilon = 0$), the right column to negative frequency dependent invasion ($\alpha_1 = 1$, $\alpha_2 = 1$, $\varepsilon = 0$). Lattice size: 80×80 . In all pictures black dots refer to species 1.

see the occurrence of small clusters based on the local feedback within the same species. For the negative frequency dependence however we observe the formation of a meander-like structure that is also known from physico-chemical structure formation [34]. It results from the antagonistic effort of each species to avoid individuals of the same kind, when being surrounded by a majority of individuals of the opposite species.

In the *stochastic* case the observed behavior strongly depends on the parameters α_1 , α_2 , ε . In particular, for *positive* frequency dependent invasion, computer simulations with different sets of parameters α_1 , α_2 show different dynamic regimes. In the example of Fig. 4, one of the species becomes extinct, i.e. the initial coexistence of both species ceases to exist in the course of time. This process is accompanied by a clustering process and eventually a segregation of both species indicated by the formation of spatial domains in Fig. 4. Fig. 5 depicts the

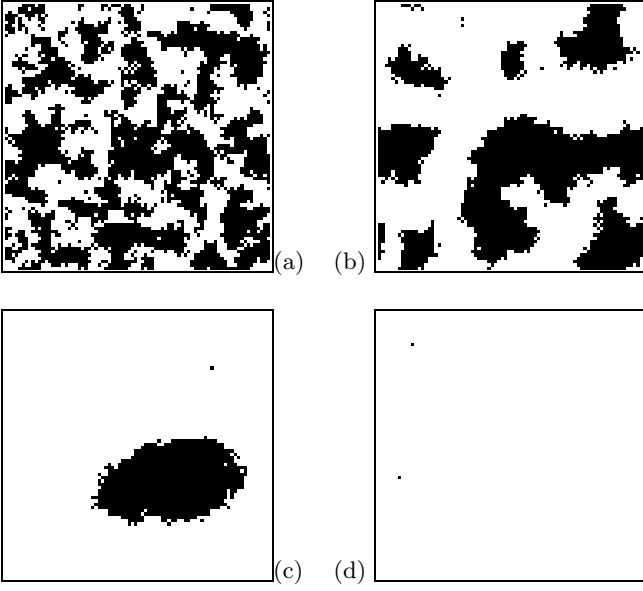


FIG. 4: Spatial snapshots of a stochastic frequency dependent invasion process with $\alpha_1 = 0.1$, $\alpha_2 = 0.3$, $\varepsilon = 10^{-4}$ (complete invasion). (a) $t = 10^1$, (b) $t = 10^2$ (c) $t = 10^3$, (d) $t = 10^4$. The initial state is equivalent to Fig. 3(a).

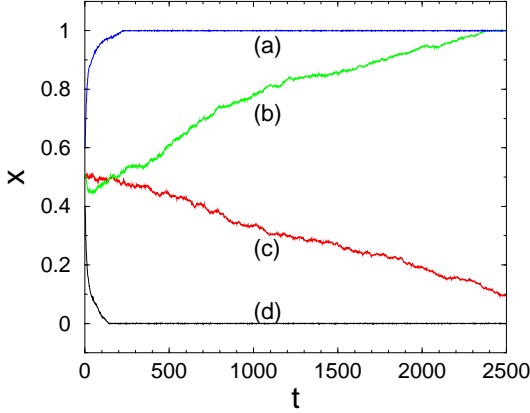


FIG. 5: Global frequency of species 1 vs. time for the same setup and parameters as in Fig. 4. The initial frequencies $x(t=0)$ of the four different runs are: (a) 0.6, (b) 0.5, (c) 0.5, (d) 0.4.

evolution of the global frequency $x(t)$ of species 1 for different initial frequencies $x(t=0)$. In every case, one species becomes extinct. For $x(t=0) > 0.5$ species 1 is the most likely survivor, while for $x(t=0) < 0.5$ it is most likely to become extinct. For $x(t=0) = 0.5$, random events during the early stage decide about its outcome. In the example of Fig. 6, obtained for another range of parameters α_1 , α_2 , we find a long-term coexistence of both species, which is accompanied by a spatial structure formation. Here, the spatial pattern remains always nonstationary and the global frequency randomly fluctuates around a mean value of $x=0.5$, as shown by

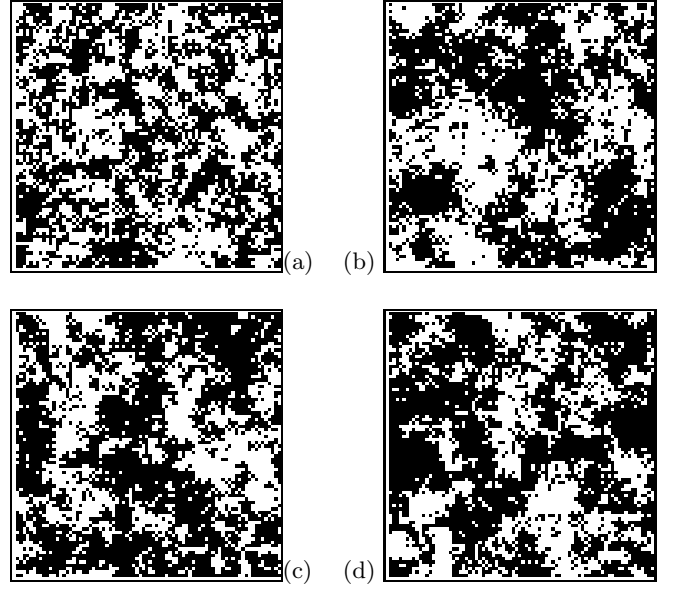


FIG. 6: Spatial snapshots of a stochastic frequency dependent invasion process with $\alpha_1 = 0.24$, $\alpha_2 = 0.30$, $\varepsilon = 10^{-4}$ (non-stationary coexistence). (a) $t = 10^1$, (b) $t = 10^2$ (c) $t = 10^3$, (d) $t = 10^4$. The initial state is equivalent to Fig. 3(a).

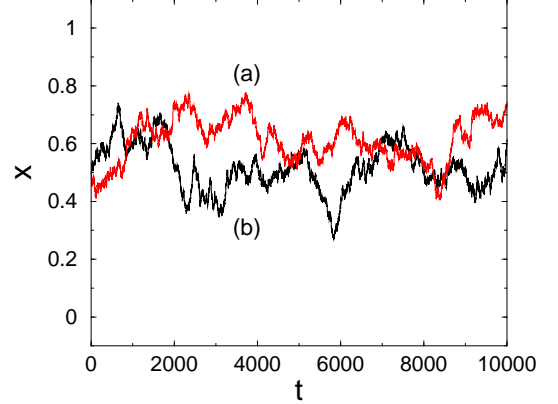


FIG. 7: Global frequency of species 1 vs. time (a) for the linear voter model, $\alpha_1 = 0.2$, $\alpha_2 = 0.4$, $\varepsilon = 10^{-4}$, and (b) for the same setup and parameters as in Fig. 6. The initial frequency is $x(t=0)=0.5$ for both runs.

Fig. 7. For yet another set of parameters, Fig. 8 shows a long-term coexistence of both species, while there are only random patterns.

For *negative* frequency dependent invasion (eq. (13)) the stochastic case shows no structures comparable to those found in the deterministic case (Fig. 3(right)). Instead, the spatial pattern remains random, similar to Fig. 8. Furthermore, regardless of the initial frequency $x(t=0)$, on a very short time scales, a global frequency $x^{\text{stat}}=0.5$ is always reached. That means we always find *coexistence* between both species. We conclude from the simulation of the CA in the stochastic case, that for *negative* frequency dependence $x^{\text{stat}}=0.5$ is the only stable value,

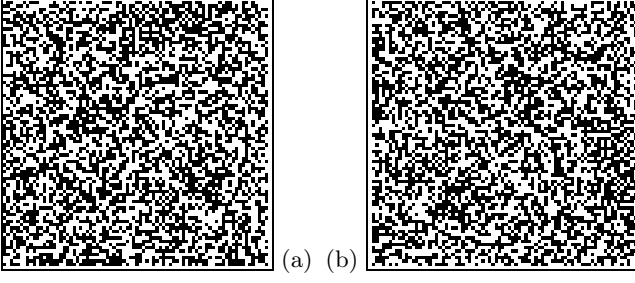


FIG. 8: Spatial snapshots of a stochastic frequency dependent invasion process with $\alpha_1 = 0.3$, $\alpha_2 = 0.4$, $\varepsilon = 10^{-4}$ (random coexistence). (a) $t = 10^1$, (b) $t = 10^5$. The initial state is equivalent to Fig. 3(a).

whereas for *positive* frequency dependence the situation is not as clear. This leads us to ask the question which ranges of α_1 , α_2 eventually lead to what kind of spatial dynamics, and how this is related to the distinction made in eq. (13). Stated otherwise: Can a dynamic leading to extinction be unambiguously assigned to a positive frequency dependence, while uniquely associating a spatial coexistence with negative frequency dependence, as done in [2]?

In order to answer these questions, in this paper we derive a phase diagram that identifies the different parameter regions and their possible dynamic regimes. In contrast to earlier investigations which restricted themselves to the mean-field limit or to pure computer simulations, we calculate our phase diagram for the *spatial* case based on *analytical approximations* of the spatial dynamics. These approximations will be compared with extensive CA simulations of the microscopic dynamics, to verify their validity. Additionally, in Sect. IIIB we also derive the phase diagram for the mean-field limit in order to allow comparison with the spatial phase diagram in Sect. V.

III. MACROSCOPIC MODEL OF INVASION

A. Derivation of the macroscopic dynamics

The key variable of the macroscopic dynamics is the global frequency $x_\sigma(t)$ of each species, defined in eq. (1). In order to compare the averaged computer simulations with results from analytical approximations in Sect. IV, we first derive an equation for the expectation value $\langle x_\sigma \rangle$. For this we start from the stochastic description given in Sect. IIB, where $p(\Theta, t)$ denoted the probability to find a particular spatio-temporal distribution Θ (eq. (2)) at time t and Θ' denoted all possible realizations of Θ eq.

(8). On one hand:

$$\begin{aligned} \langle x_\sigma(t) \rangle &= \frac{1}{N} \sum_{\Theta'} \left(\sum_{i=1}^N \delta_{\sigma\theta_i} \right) p(\Theta', t) \\ &= \frac{1}{N} \sum_{\Theta'} N_\sigma p(\Theta', t) = \frac{\langle N_\sigma(t) \rangle}{N} \end{aligned} \quad (14)$$

and on the other hand:

$$\begin{aligned} \langle x_\sigma(t) \rangle &= \frac{1}{N} \sum_{i=1}^N \sum_{\Theta'} \delta_{\sigma\theta_i} p(\Theta', t) \\ &= \frac{1}{N} \sum_{i=1}^N p_i(\theta_i = \sigma, t) \end{aligned} \quad (15)$$

By differentiating eq. (15) with respect to time and inserting the master eq. (10), we find the following macroscopic dynamics for the CA:

$$\begin{aligned} \frac{d}{dt} \langle x_\sigma(t) \rangle &= \frac{1}{N} \sum_{i=1}^N \sum_{\underline{\theta}'_i} \left[w(\sigma|(1-\sigma), \underline{\theta}'_i) \times \right. \\ &\quad \times p(\theta_i = (1-\sigma), \underline{\theta}'_i, t) \\ &\quad \left. - w(1-\sigma|\sigma, \underline{\theta}'_i) p(\theta_i = \sigma, \underline{\theta}'_i, t) \right] \end{aligned} \quad (16)$$

For the further treatment of eq. (16), we consider a specific distribution of states on $n = m + 1$ cells defined by $\underline{\sigma}^0$. This distribution is assigned to a particular neighborhood of cell i by $\eta_i^0(\underline{\sigma}^0)$ (eq. (5)). Since we are interested in how many times a special realization of a specific distribution $\underline{\sigma}^0$ is present in the population, we define an indicator function

$$\chi(\underline{\eta}_i^0) \equiv \chi_{\underline{\sigma}^0}(\eta_i^0(\underline{\sigma}^0)) = \delta_{\underline{\eta}_i, \underline{\sigma}^0} \quad (17)$$

that is 1 if the neighborhood of cell i has the distribution $\underline{\sigma}^0$, and 0 otherwise. Therefore, we write the frequency of the n -tuple $\underline{\sigma}^0$ in the population as:

$$x_{\underline{\sigma}^0}(\Theta) := \frac{1}{N} \sum_{i=1}^N \chi(\underline{\eta}_i^0) \quad (18)$$

The expectation value is

$$\langle x_{\underline{\sigma}^0}(t) \rangle = \sum_{\Theta'} x_{\underline{\sigma}^0}(\Theta') p(\Theta', t) \quad (19)$$

Inserting eq. (18) into eq. (19), we verify that

$$\begin{aligned} \langle x_{\underline{\sigma}^0}(t) \rangle &= \frac{1}{N} \sum_{i=1}^N \sum_{\Theta'} \chi(\underline{\eta}_i^0) p(\Theta', t) \\ &= \frac{1}{N} \sum_{i=1}^N p(\underline{\eta}_i^0, t) \end{aligned} \quad (20)$$

because of the definition of the marginal distribution. Using the identity $p(\underline{\eta}_i^0, t) = p(\sigma, \underline{\eta}_i, t)$, we may rewrite

eq. (16) by means of eq. (20) to derive the macroscopic dynamics in the final form:

$$\frac{d}{dt} \langle x_\sigma(t) \rangle = \sum_{\underline{\sigma}'} \left[w(\sigma|1-\sigma, \underline{\sigma}') \langle x_{(1-\sigma), \underline{\sigma}'}(t) \rangle - w(1-\sigma|\sigma, \underline{\sigma}') \langle x_{\sigma, \underline{\sigma}'}(t) \rangle \right] \quad (21)$$

$\underline{\sigma}'$ denotes the 2^m possible configurations of a specific occupation distribution $\underline{\sigma}$ (eq. (4)). In the following, we use $\langle x \rangle \equiv \langle x_1 \rangle = 1 - \langle x_0 \rangle$. Then, the dynamic for $\langle x \rangle$ reads:

$$\frac{d}{dt} \langle x(t) \rangle = \sum_{\underline{\sigma}'} \left[w(1|0, \underline{\sigma}') \langle x_{0, \underline{\sigma}'}(t) \rangle - w(0|1, \underline{\sigma}') \langle x_{1, \underline{\sigma}'}(t) \rangle \right] \quad (22)$$

The solution of eq. (22) would require the computation of the averaged global frequencies $\langle x_{1, \underline{\sigma}} \rangle$ and $\langle x_{0, \underline{\sigma}} \rangle$ for all possible occupation patterns $\underline{\sigma}$, which would be a tremendous effort. Therefore, in Sect. III C we will introduce an analytical approximation to solve this problem. In Sect. IV A we will further show by means of computer simulations that this approximation is able to describe the averaged dynamics of the CA. Before we come to this, we investigate the mean-field limit of the macroscopic dynamics. This will provide us on one hand with a first understanding of the parameter dependence of the model, and on the other hand allows further comparison with the spatial case.

B. Investigation of the mean-field limit

In the mean-field limit the state of each cell does not depend on the occupation distribution of its four neighbors, but on four randomly chosen sites. In this case the occupation distribution factorizes:

$$\langle x_{\underline{\sigma}^0} \rangle = \langle x_\sigma \rangle \prod_{j=1}^m \langle x_{\sigma_j} \rangle \quad (23)$$

For the macroscopic dynamics (eq. (22)) we find:

$$\frac{d}{dt} \langle x(t) \rangle = \sum_{\underline{\sigma}'} \left[w(1|0, \underline{\sigma}') (1 - \langle x \rangle) \prod_{j=1}^m \langle x_{\sigma_j} \rangle - w(0|1, \underline{\sigma}') \langle x \rangle \prod_{j=1}^m \langle x_{\sigma_j} \rangle \right] \quad (24)$$

For the calculation of the $\langle x \rangle_{\sigma_j}$ we have to look at each possible occupation pattern $\underline{\sigma}$ for a neighborhood $m=4$. For instance, $\underline{\sigma}^0 = \{10010\}$. The mean-field approach assumes that the occurrence of each 1 or 0 in the pattern can be described by the global frequencies x and $(1-x)$, respectively (for simplicity, the abbreviation $x \equiv \langle x \rangle$ will be used in the following). For the previous example of

string $\underline{\sigma}^0 = \{10010\}$ we find $\langle x_{\underline{\sigma}^0} \rangle = x^2(1-x)^3$. Inserting eq. (12) for the transition rates, we find the equation for the mean-field dynamics to be:

$$\begin{aligned} \frac{dx}{dt} = \varepsilon & \left[(1-x)^5 - x^5 \right] + x^5 - x + x(1-x)^4 (5\alpha_1) \\ & + x^2(1-x)^3 (10\alpha_2) + x^3(1-x)^2 [10(1-\alpha_2)] \\ & + x^4(1-x) [5(1-\alpha_1)] \end{aligned} \quad (25)$$

The fixed points of the mean-field dynamics can be calculated from eq. (25) using $\dot{x} = 0$. In the limit $\varepsilon = 0$, we find:

$$\begin{aligned} x^{(1)} &= 0; & x^{(2)} &= 1; & x^{(3)} &= 0.5 \\ x^{(4,5)} &= 0.5 \pm \sqrt{\beta_1/4\beta_2} \\ \beta_1 &\equiv \alpha_2 + 1.5\alpha_1 - 0.7; & \beta_2 &\equiv \alpha_2 - 0.5\alpha_1 - 0.3 \end{aligned} \quad (26)$$

The first three stationary solutions denote either a complete extinction of one species or an equal share of both of them. “Nontrivial” solutions, i.e. a *coexistence* of both species with different shares of the total population, can only result from $x^{(4,5)}$, provided that the solutions are (i) real and (ii) in the interval $\{0, 1\}$. The first requirement means that the two functions β_1, β_2 are either both positive or both negative. The second requirement additionally results in $\alpha_1 \leq 0.2$ if $\alpha_2 \geq 0.4$ and $\alpha_1 \geq 0.2$ if $\alpha_2 \leq 0.4$. This leads to the phase diagram of the mean-field case shown in Fig. 9.

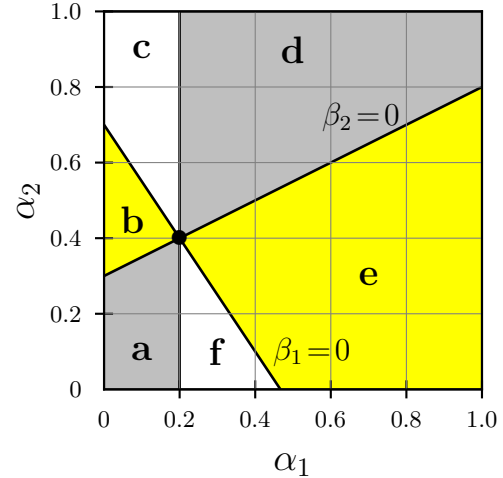


FIG. 9: Phase diagram of the invasion dynamics in the mean-field case. For the different areas see text. The functions $\beta_1 = 0$ and $\beta_2 = 0$ are given by eq. (26). The areas in lighter gray indicate imaginary solutions of $x^{(4,5)}$, eq. (26) while the areas in darker gray indicate solutions of $x^{(4,5)}$ outside the $\{0, 1\}$ interval. The linear voter point is indicated by •

In order to verify the stability of the solutions, we have further investigated the Jacobian d/dx of eq. (25). The results can be summarized as follows:

- In the regions *a* and *b* of the mean-field phase diagram, Fig. 9, $x^{\text{stat}} = 0$ and $x^{\text{stat}} = 1$ are the only stable fixed points of the dynamics, while $x = 0.5$ is

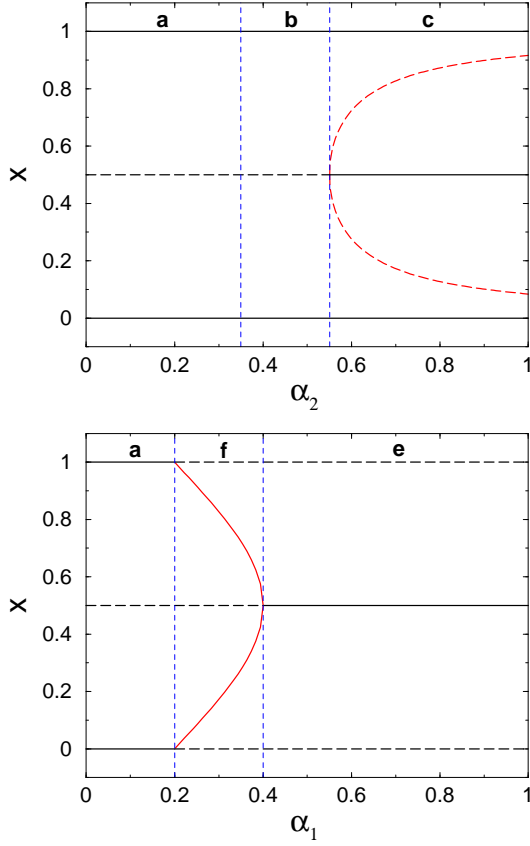


FIG. 10: Bifurcation diagram of the stationary solutions dependent on α_1 and α_2 . (top) $\alpha_1 = 0.1$, (bottom) $\alpha_2 = 0.1$. The solid lines refer to stable solutions, the dashed lines to unstable ones. The notations a-f refer to the respective areas in the phase diagram, Fig. 9.

an unstable fixed point (cf. also Fig. 10top). Species 1 with $x(t=0) < 0.5$ will most likely become extinct, while it will remain as the only survivor for $x(t=0) > 0.5$. Thus, the region (a, b) can be characterized as the region of *extinction*.

- In region c, the mean-field limit predicts the three stable fixed points 0, 1 and 0.5. The attractor basin for 0.5 is the largest as Fig. 10(top) indicates. The separatrices are given by the unstable solutions $x^{(4,5)}$, eq. (26). In this parameter region, the mean-field limit predicts either *coexistence* of both species with equal shares, or *extinction* of one species, dependent on the initial condition $x(t=0)$.
- In the regions d and e, only one stable fixed point $x^{\text{stat}} = 0.5$ can be found, while the solutions 0 and 1 are unstable (cf. also Fig. 10bottom). Thus, the mean-field approach predicts the *coexistence* of both species with equal share.
- Finally, in region f the solutions 0, 1 and 0.5 are

unstable fixed points, but the two remaining solutions $x^{(4,5)}$, eq. (26) are stable fixed points (cf. Fig. 10bottom). Thus, this region is the most interesting one, since it seems to enable “nontrivial” solutions, i.e. an *asymmetric coexistence* of both species with different shares. We note again, that this is a prediction of the mean-field analysis. At the intersection of regions f and a, these two solutions approach 0 and 1, while at the intersection of regions f and e they both converge to 0.5.

C. Pair approximation of spatial effects

So far, we have investigated the mean-field case based on the approximation of eq. (23). In order to solve the macroscopic eq. (22) with respect to *spatial correlations*, another analytical approximation will be discussed in this section. This is the so-called *pair approximation* that is based on the assumption that the state θ_i of each cell i is only correlated to the states θ_{ij} of its nearest neighbors (eq. (3)) as described in Fig. 1. In pair approximation, we are not interested in the occupation distribution of a whole neighborhood $\underline{\sigma}^0$ (eq. (5)) but only in *pairs* of nearest neighbor cells, σ, σ' with $\sigma' \in \{0, 1\}$. That means, that the local neighborhood of nearest neighbors is decomposed into pairs, i.e. blocks of size 2 that are called *doubelets*.

Similar to eq. (18), the global frequency of doubelets is defined as:

$$x_{\sigma, \sigma'} = \frac{1}{N} \sum_{i=1}^N \sum_{j=1}^m \frac{1}{m} \chi(\theta_i = \sigma, \theta_{ij} = \sigma') \quad (27)$$

The expected value of the doublet frequency is then given by $\langle x_{\sigma, \sigma'} \rangle$ in the same way as in eq. (19). We now define the correlation term as:

$$c_{\sigma|\sigma'} := \frac{\langle x_{\sigma, \sigma'} \rangle}{\langle x_{\sigma'} \rangle} \quad (28)$$

neglecting higher order correlations. Thus $c_{\sigma|\sigma'}$ can be seen as an approximation of the conditional probability that a randomly chosen nearest neighbor of a cell in state σ' is in state σ . Using the above definitions, we have the following relations:

$$\langle x_{\sigma'} \rangle c_{\sigma|\sigma'} = \langle x_{\sigma} \rangle c_{\sigma'|\sigma}; \quad \sum_{\sigma' \in \{0,1\}} c_{\sigma|\sigma'} = 1 \quad (29)$$

For the case of two species $\sigma \in \{0, 1\}$, $c_{1|1}$ and $c_{0|0}$ are the *inter-species* correlations, while $c_{1|0}$ and $c_{0|1}$ denote the *intra-species* correlations. Using $\langle x \rangle \equiv \langle x_1 \rangle$, these correlations can be expressed in terms of only $c_{1|1}$ and

$\langle x \rangle$ as follows:

$$\begin{aligned} c_{0|1} &= 1 - c_{1|1} \\ c_{1|0} &= \frac{\langle x \rangle (1 - c_{1|1})}{1 - \langle x \rangle} \\ c_{0|0} &= \frac{1 - 2\langle x \rangle + \langle x \rangle c_{1|1}}{1 - \langle x \rangle} \end{aligned} \quad (30)$$

Now, the objective is to express the global frequency of a specific occupation pattern $\langle x_{\underline{\sigma}^0} \rangle$ (eq. (19)) in terms of the correlation terms $c_{\sigma|\sigma'}$. In pair approximation, it is assumed that the states θ_{i_j} are correlated only through the state θ_i and uncorrelated otherwise. Then the global frequency terms in eq. (21) can be approximated as follows:

$$\langle x_{\underline{\sigma}^0} \rangle = \langle x_{\sigma} \rangle \prod_{j=1}^m c_{\sigma_j|\sigma} \quad (31)$$

For the macroscopic dynamics (eq. (22)) we find in pair approximation:

$$\begin{aligned} \frac{d}{dt} \langle x(t) \rangle &= \sum_{\underline{\sigma}'} \left[w(1|0, \underline{\sigma}') (1 - \langle x \rangle) \prod_{j=1}^m c_{\sigma_j|\sigma} \right. \\ &\quad \left. - w(0|1, \underline{\sigma}') \langle x \rangle \prod_{j=1}^m c_{\sigma_j|(1-\sigma)} \right] \end{aligned} \quad (32)$$

Note that the $c_{\sigma_j|\sigma}$ can be expressed in terms of $c_{1|1}$ by means of eq. (30). Thus, eq. (32) now depends on only two variables, $\langle x \rangle$ and $c_{1|1}$. In order to derive a *closed* form description, we need an additional equation for $\dot{c}_{1|1}$. That can be obtained from eq. (28):

$$\frac{dc_{1|1}}{dt} = -\frac{c_{1|1}}{\langle x \rangle} \frac{d}{dt} \langle x \rangle + \frac{1}{\langle x \rangle} \frac{d}{dt} \langle x_{1,1} \rangle \quad (33)$$

Eq. (33) also requires the time derivative of the global doublet frequency $\langle x_{1,1} \rangle$. In the Appendix, these three equations are explicitly derived for the neighborhood $m = 4$ using the transition rates of eq. (12).

Even in their lengthy form, the three eqs. (A1), (A6), (A7) can easily be solved numerically. In the next section, we will show that they yield some characteristic quantities such as $\langle x(t) \rangle$ also in the spatial case in very good agreement with the results of the CA simulations.

IV. SIMULATION RESULTS

A. Global frequencies and spatial correlations

In this section, we investigate how well the pair approximation, eqs. (A1), (A6), (A7) of the spatial macroscopic dynamics (eq. (22)) predict the global quantities of the CA. For comparison, we conduct microscopic computer simulations of the CA, calculate the quantities of interest

and average them over 50 runs. The results for the global frequency $\langle x \rangle$ and the spatial correlation $c_{1|1}$ are plotted in Fig. 11 for the case of complete invasion, also shown in Fig. 4, and in Fig. 12 for the case of coexistence.

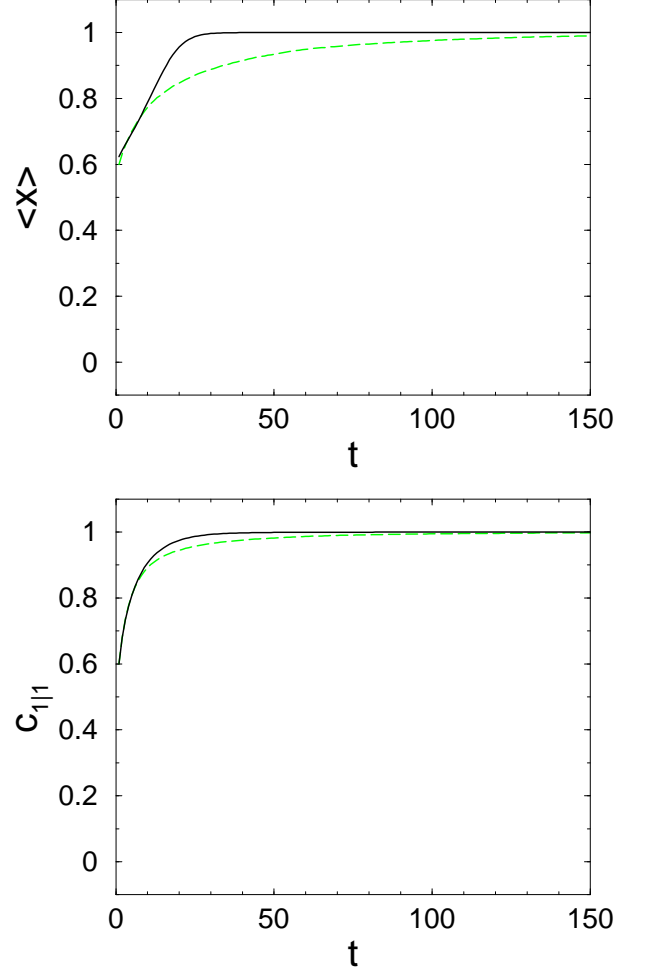


FIG. 11: Global frequency $\langle x \rangle$ and spatial correlation $c_{1|1}$ for the case of complete invasion. Solid line: pair approximation, dashed line: CA simulations, averaged over 50 runs. Parameters and spatial snapshots see Fig. 4.

The figures demonstrate that, after some initial differences, the global frequencies $\langle x \rangle$ can be described by the pair approximation for the asymptotic limit for *both* cases of complete invasion and coexistence. The approximation of the spatial correlation $c_{1|1}$ is accurate only for the case of complete invasion, but shows some deviations for the case of random coexistence. We have tested the latter case for various parameter values and found values for $c_{1|1}$ between 0.4 and 0.6, compared to $c_{1|1} = 0.5$ from the CA simulation. The discrepancy is understandable, since in the case of long-term coexistence the spatial patterns change *very frequently* between different random configurations. Thus, while the global frequency settles down to 0.5, the dynamics is still non-stationary. For the case of spatial domain formation long-range correlations

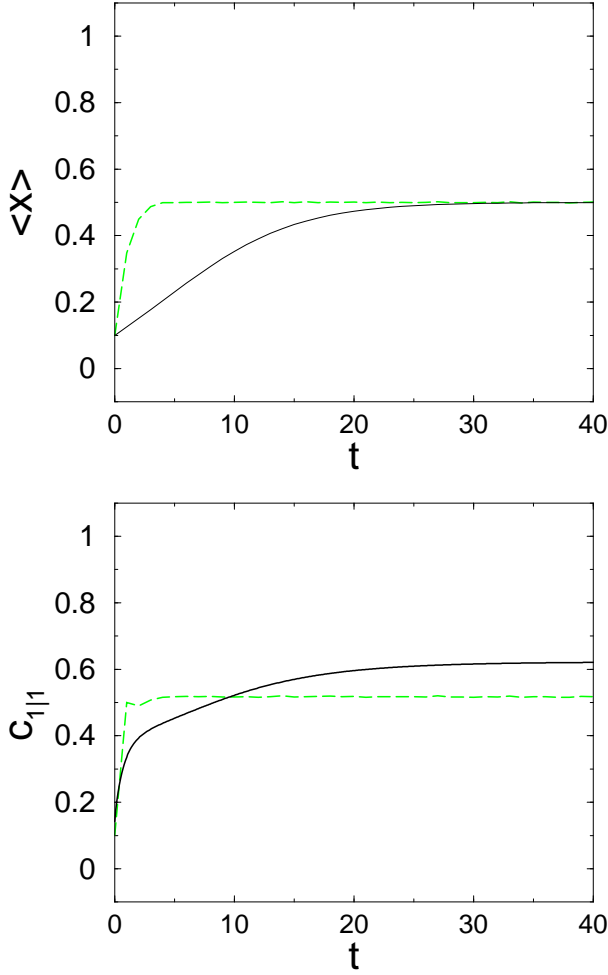


FIG. 12: Global frequency $\langle x \rangle$ and spatial correlation $c_{1|1}$ for the case of random coexistence. Solid line: pair approximation, dashed line: CA simulations, averaged over 50 runs. Parameters and spatial snapshots see Fig. 8.

exist that can be described well by the pair approximation, but this fails for the short-range correlations of the random patterns.

B. Vector plots of macroscopic dynamics

In order to find the different attractors of the macroscopic dynamics, it is useful to look at the possible trajectories in the state space of the global frequency $\langle x \rangle$ and the spatial correlation $c_{1|1}$. These two variables are described in pair approximation by Eqs. (A1), (A7). The vector plots in Fig. 13 show the mutual change of $\langle x \rangle$ and $c_{1|1}$ by means of arrows. We have used a linear transformation of the magnitude of $d\vec{x} + dc_{1|1}$, so that vector lengths near zero are still represented by visible arrows, to illustrate the direction. The plots tell us how the macroscopic dynamics will evolve for given initial conditions.

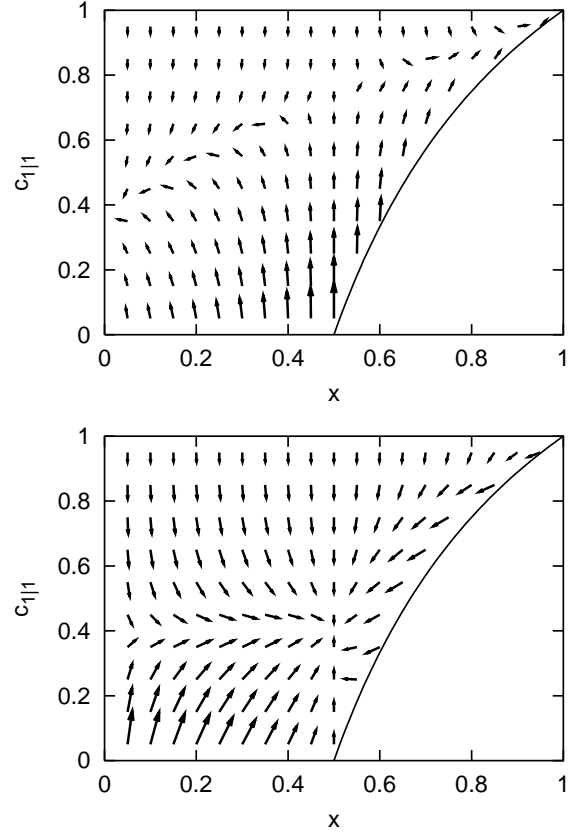


FIG. 13: Vector plots of macroscopic dynamics for invasion dynamics ($\alpha_1 = 0.1, \alpha_2 = 0.3, \varepsilon = 10^{-4}$) (top) and long-term coexistence ($\alpha_1 = 0.9, \alpha_2 = 0.7, \varepsilon = 10^{-4}$) (bottom)

For the case of complete invasion (Fig. 13 (top)), the dynamics leads towards the attractor $\{\langle x \rangle, c_{1|1}\} = \{1, 1\}$, or $\{0, 0\}$ (note that the arrows pointing to $\{0, 0\}$ for small $\langle x \rangle$ are not shown in the figure). This is in agreement with the results of the CA microsimulations shown in Figs. 4, 5. As can be observed in Fig. 13 (top), the two attractor basins are separated by $\langle x \rangle = 0.5$. For negative frequency dependence (Fig. 13 (bottom)) the dynamics lead to the only attractor $\{\langle x \rangle, c_{1|1}\} = \{0.5, 0.4\}$, where the CA microsimulation yields $\{0.5, 0.5\}$. The difference in $c_{1|1}$ results from the limitation of the pair approximation for this case, as explained above.

The two vector plots in Fig. 13 also show a region in the state space that is not reached by the dynamics. We found that the boundary of the attainable region can be described as:

$$0 \leq c_{1|1} \leq 1 \quad \text{if} \quad 0 \leq \langle x \rangle \leq 0.5$$

$$2 - \frac{1}{\langle x \rangle} \leq c_{1|1} \leq 1 \quad \text{if} \quad 0.5 \leq \langle x \rangle \leq 1 \quad (34)$$

The boundary of this region can be explained as follows: As long as $\langle x \rangle(t=0) < 0.5$, $c_{1|1}(t=0)$ can take values in the range of $\{0, 1\}$. However, as $\langle x \rangle(t=0)$ exceeds 0.5, it is obvious that some lower values of $c_{1|1}$ are not possible. Consider a 2-dimensional lattice of $N = N_0 + N_1$ cells and

$x \geq 0.5$. Then, the lower limit of the number N_{11} of pairs (1,1) is $N_{11} \geq 2N - 2N_0$, since every cell has 4 neighbors and each $\theta_i = 0$ can lead to up to 4 non-(1,1) pairs. The minimal value is obtained for $\theta_{i_j} \neq 0$ ($j = 1, \dots, m$). For example, with $x = 0.5$, the cells must be arranged in a checkerboard manner in order to reach the minimal x_{11} . Thus, we have

$$c_{1|1} = \frac{x_{11}}{x} = \frac{1}{x} \frac{N_{11}}{2N} \geq \frac{1}{x} \frac{2N - 4(N - N_1)}{2N} = 2 - \frac{1}{x} \quad (35)$$

V. PHASE DIAGRAM

The CA simulations in Sect. 2 have shown that dependent on the parameters α_1 and α_2 three different dynamic regimes can be observed that are related to different kinds of spatio-temporal pattern formation: (i) complete invasion of one of the species via the formation of large spatial domains, (ii) long-term coexistence of both species with random distribution, (iii) long-term coexistence of both species with formation of non-stationary domains.

In order to find the boundaries in parameter space between these different regimes, i.e. to derive a *phase diagram*, we carry out CA simulations of the complete parameter space, $0 \leq (\alpha_1, \alpha_2) \leq 1$. The outcome of these simulations is averaged and compared to the asymptotic solutions of the dynamic equations (A1), (A7) which result from the pair approximation. The phase diagram shown in Fig. 14 should be compared to Fig. 9, which results from the mean-field analysis in Sect. IIIB and thus neglects any kind of spatial correlation.

Instead of the six regions distinguished in the mean-field phase diagram (Fig. 9) in the spatial case we can distinguish *two* different regions divided by one separatrix:

1. The parameter region left of the separatrix refers to the *complete invasion* of one of the species, with *high* spatial correlations during the evolution. The dynamics of the macroscopic variables for this case are shown in Fig. 11. In the CA simulations, we observe the formation of domains that grow in the course of time until exclusive domination prevails (cf. Fig. 4). Asymptotically, a *stationary* pattern is observed, with $\langle x \rangle = 1$ (or 0) and $c_{1|1} = 1$ (or 0).
2. The region to the right of the separatrix refers to *random spatial coexistence* of both species with $\langle x \rangle = 0.5$ and *no* spatial correlations, i.e. $c_{1|1} = 0.5$. The dynamics of the macroscopic variables for this case are shown in Fig. 12. In the CA simulations, we observe *non-stationary* random patterns that change with high frequency (cf. Fig. 8).

Both regions are divided by a separatrix that has in fact a certain extension in the parameter space. As shown in Fig. 14, the separatrix is divided into two pieces by the linear voter point, (0.2;0.4). Above that point, the

separatrix is simply a line, but below the voter point the extension in parameter space becomes noticeable.

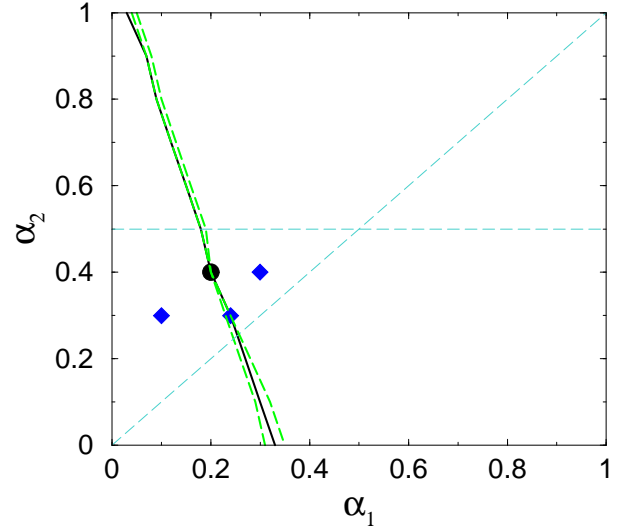


FIG. 14: Phase diagram of the invasion dynamics in the spatial case. Solid line: pair approximation, dashed line: CA simulations, averaged over 50 runs. The linear voter point (0.2,0.4) is indicated by \bullet . Further, \diamond marks those three parameter sets where results of computer simulations are shown for (i) the spatial evolution (Figs. 4, 6, 8) and (ii) for the global frequency $\langle x \rangle$ and the spatial correlation $c_{1|1}$ (Figs. 7, 11, 12, 15, 16). The straight dashed lines mark the different parameter areas given in eq. (13) which are also shown in Fig. 2.

Looking at the dynamics *on* the separatrix, we find in Fig. 15 that the mean frequency is $\langle x \rangle = 0.5$ both above and below the voter point. The spatial correlation $c_{1|1}$ is 0.5 above the voter point, but 0.7 below the voter point as Fig. 16 shows. $c_{1|1} = 0.7$ holds within the whole extended area of the separatrix and can be confirmed by the spatial analysis. For example, below the voter point, going over from the right to the left side of the phase diagram, we notice a transition from 0.5 to 1.0 in the mean frequency, and from 0.5 to 0.7 to 1.0 in the spatial correlations. Thus, in fact $c_{1|1}$ separates the two dynamic regimes (below the voter point). For parameters chosen from the separatrix in that region, we find a long-term and non-stationary *coexistence* between the two species as on the *right* side of the phase diagram. But we also find the long-range spatial correlations that lead to the formation of spatial domains as shown e.g. in Fig. 6 – which is characteristic for the *left* side of the phase diagram. The spatial pattern formation is also indicated by large fluctuations of $\langle x \rangle$ shown in Fig. 15(top) compared to Fig. 15(bottom). A single run, as shown in Fig. 7, clearly indicates the long-term non-stationary coexistence of both species.

We emphasize that the separatrix between the two dynamic regimes is well predicted by the macroscopic dynamics resulting from the pair approximation (as can be clearly seen in Fig. 14). Comparing the phase diagram for

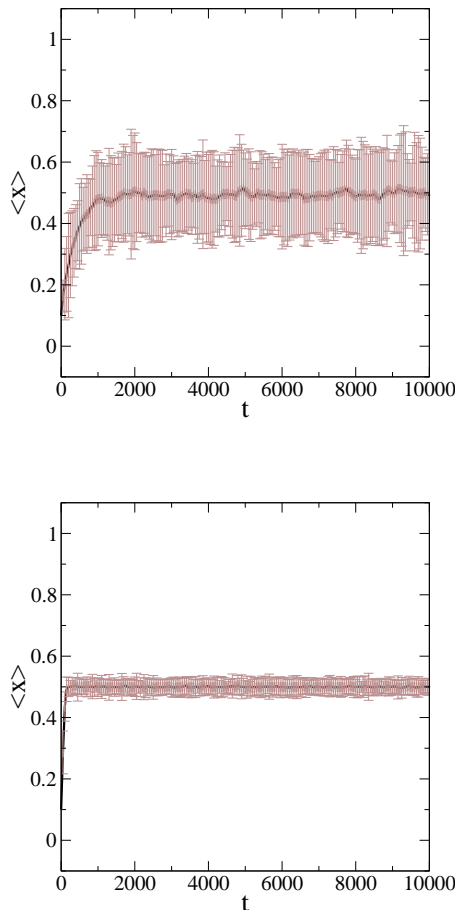


FIG. 15: Global frequency $\langle x \rangle$ with min-max deviations averaged over 50 CA simulations. The parameters are picked from the *separatrix* shown in Fig 14: (top) $(\alpha_1, \alpha_2) = (0.24, 0.3)$ (below the voter point, see also Figs. 6, 7), (bottom) $(\alpha_1, \alpha_2) = (0.11, 0.80)$ (above the voter point).

the spatial case with the one obtained from the mean-field approximation, we realize that the most interesting regions in Fig. 9, namely (c) and (f), have simply collapsed into the separatrix shown in Fig. 14. While the region of unstable asymmetric coexistence, (c), relates to the separatrix line above the voter point, the region of stable asymmetric coexistence, (f), relates to the extended area of the separatrix shown below the voter point in Fig. 14.

We conclude that in the spatial case, no regions of stationary *and* asymmetric coexistence between the two species exist, as was predicted by the mean-field analysis. However, we find a (small but extended) region *on* the separatrix that shows the *non-stationary* and asymmetric coexistence of the two species for *single* realizations (which results in a symmetric coexistence, $\langle x \rangle = 0.5$).

Finally, looking at the phase diagram (Fig. 14) we realize that the distinction made in eq. (13) based on α_1, α_2 is not necessarily related to the spatial dynamics ob-

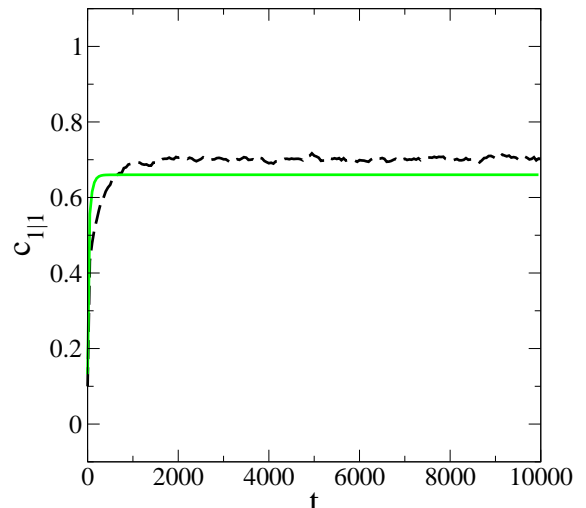


FIG. 16: Spatial correlation $c_{1|1}$ for the simulations shown in Fig. 15 (top) (cf. also Fig. 6). Solid line: pair approximation, dashed line: CA simulations, averaged over 50 runs.

served. In particular, a random coexistence can be found for *negative* frequency dependent dynamics as well as for *positive* frequency dependence, which was so far assigned to complete invasion only [2]. On the other hand, complete invasion is not observed only for positive frequency dependence, but also for positive and negative allee effects. A random spatial coexistence can be found for positive and negative allee dynamics as well. The only case where just one dynamic regime can be observed is the case of negative frequency dependence. We note, however, that the nonstationary long-term coexistence with spatial pattern formation occurs both for the positive frequency dependence and the negative allee dynamics, given that the parameters are chosen from the most interesting zone of the separatrix below the voter point.

VI. CONCLUSIONS

In this paper, we investigated a cellular automaton that models the frequency-dependent dynamics of two species $\{0, 1\}$ in a spatial environment. The basic assumption for the microscopic dynamics is that the probability to occupy a given cell with either species 0 or 1 depends on the frequency of this species in the immediate neighborhood.

In a formal approach, this dynamic is described by the so-called non-linear voter model that has been previously investigated by means of computer simulations [2], mean-field analysis and Markov analysis [28]. Our contribution to this problem is an analytical investigation of the spatial model by means of a pair approximation of the macroscopic dynamics. Differing from previous in-

vestigations, we present for the first time a closed formal description of the two-dimensional spatial problem. In order to compare the predictions of the analytical approach with microscopic computer simulations, we have (i) derived a macroscopic dynamics for the global frequency x_σ of each species in the total population, eq. (21) and (ii) investigated this dynamics on two different levels of approximation, the mean-field limit, eq. (23) and the pair approximation, eq. (31). In our paper, the mean-field approximation plays the role of a reference state used to demonstrate the differences of the spatial case.

Using pair approximation we were able to derive a set of two coupled time-dependent equations that describe the macroscopic spatial dynamics in terms of the global frequency $\langle x \rangle$ (eq. (32)) and the spatial correlation $c_{1|1}$ (eq. (33)). These equations can be solved numerically and can be compared with results of the averaged simulations of the full CA. As shown in detail in Sect. IV, the global frequency $\langle x \rangle$ is accurately predicted by the pair approximation both for the invasion dynamics and the coexistence regime, while the spatial correlation $c_{1|1}$ shows some deviations from the simulation results in the coexistence regime. Despite this, the pair approximation is a valuable tool, particularly with respect to computational efforts. The simulations of the CA are more timeconsuming, since the results of the different runs have to be averaged afterwards. The pair approximation, on the other hand, is based on only 2 coupled equations and therefore needs less computational effort.

In particular, the pair approximation has shown its advantages in the calculation of the spatial phase diagram shown in Fig. 14. The derivation of the phase diagram based on such analytical approaches is considered a major result of this paper. While a distinction is usually made in the parameter space in terms of positive and negative frequency dependence, and positive and negative allee effects, eq. (13) and Fig. 2, we were able to show in our analysis that this has no effect on the spatial dynamics. Instead, based on the pair approximation, we verified that only two different regimes exist for the frequency dependent dynamics of the CA: We found (i) a segregation between the two species, leading to the formation of large domains on intermediate time scales and to an extinction of one of the species asymptotically, and (ii) a long-term coexistence of both species with no spatial correlations. Both regimes are separated by the separatrix that was predicted well by pair approximation. The most interesting dynamic, where both spatial structures and non-stationary coexistence on long time scales is found, was observed for parameters chosen from the separatrix below the voter point. This narrow region accounts for nontrivial asymptotic behavior. But even in this region, variables of the global dynamics such as the average frequency or the spatial correlations can be reproduced by means of the pair approximation – thus the efforts of deriving a closed analytical description pays off, indeed.

Acknowledgments

The authors want to thank Thilo Mahnig for discussions on Sect. III.

APPENDIX A

Here we derive some explicit expressions for the three equations of the pair approximation discussed in Sect. III C, for the global frequency $\langle x \rangle$ (eq. (32)), the doublet frequency $\langle x_{1,1} \rangle$ and the correlation term $c_{1|1}$ (eq. (33)). The equations are derived for the neighborhood $m = 4$. We use the notation $x \equiv \langle x \rangle$. Using eq. (30) and the transition rates of eq. (12), we find for $\langle x \rangle$, eq. (32) in pair approximation:

$$\begin{aligned} \frac{dx}{dt} = & \varepsilon \left[\frac{1}{(1-x)^3} (1-2x+xc_{1|1})^4 - xc_{1|1}^4 \right] \\ & + 4\alpha_1 \left[\frac{x}{(1-x)^3} (1-2x+xc_{1|1})^3 (1-c_{1|1}) \right. \\ & \quad \left. - x(1-c_{1|1})c_{1|1}^3 \right] \\ & + 6\alpha_2 \left[\frac{x^2}{(1-x)^3} (1-2x+xc_{1|1})^2 (1-c_{1|1})^2 \right. \\ & \quad \left. - x(1-c_{1|1})^2 c_{1|1}^2 \right] \\ & + (1-\alpha_1) \left[\frac{x^4}{(1-x)^3} (1-c_{1|1})^4 - x(1-c_{1|1})^4 \right] \\ & + 4(1-\alpha_2) \left[\frac{x^3}{(1-x)^3} (1-2x+xc_{1|1})(1-c_{1|1})^3 \right. \\ & \quad \left. - x(1-c_{1|1})^3 c_{1|1} \right] \end{aligned} \quad (\text{A1})$$

We note that $c_{1|1} = c_{1|0} = x$ and $c_{0|0} = c_{0|1} = 1-x$ in the mean-field limit, in which case eq. (A1) reduces to eq. (25).

In order to calculate the time derivative of the doublet frequency $\langle x_{1,1} \rangle$ we have to consider how it is affected by changes of σ in a specific occupation pattern of size $m = 4$, $\underline{\sigma}^0 = \{\sigma, \sigma_1, \sigma_2, \sigma_3, \sigma_4\}$, considering the σ_j as constant. Again, in a frequency dependent process it is assumed that the transition does not depend on the exact distribution of the σ_j , but only on the frequency of a particular state σ in the neighborhood. Let $S_{\sigma,q}$ describe a neighborhood where the center cell in state σ is surrounded by q cells of the same state σ . For any given $q \leq m$, there are $\binom{m}{q}$ such occupation patterns. The global frequency of neighborhood $S_{\sigma,q}$ is denoted as $x_{\sigma,q}$ with the expectation value $\langle x_{\sigma,q} \rangle$. Obviously, $x_{\sigma,q}$ can be calculated from the global frequencies $x_{\sigma,\underline{\sigma}'}$ of all possible occupation distributions $\underline{\sigma}'$ (eq. (4)), that match the condition

$$z^\sigma = \sum_{j=1}^m \delta_{\sigma,\sigma_j} := q \quad (\text{A2})$$

i.e. it is defined as

$$x_{\sigma,q} = \sum_{\underline{\sigma}', z^{\sigma'}=q} x_{\sigma,\underline{\sigma}'} \quad (\text{A3})$$

Regarding the possible transitions, we are only interested in changes of the doublet (1,1), i.e. transitions (1,1) \rightarrow (0,1) or (0,1) \rightarrow (1,1). The transition rates shall be denoted as $w((0,1)|(1,1), S_{\sigma,q})$ and $w((1,1)|(0,1), S_{\sigma,q})$ respectively, which of course depend on the local neighborhood $S_{\sigma,q}$. With this, the dynamics of the expected doublet frequency can be described by the rate equation:

$$\begin{aligned} \frac{d}{dt} \langle x_{1,1} \rangle (t) = \sum_{q=0}^m & \left[w((1,1)|(0,1), S_{0,q}) \langle x_{0,q} \rangle \right. \\ & \left. - w((0,1)|(1,1), S_{1,q}) \langle x_{1,q} \rangle \right] \end{aligned} \quad (\text{A4})$$

In order to specify the transition rates of the doublets $w((\sigma',1)|(\sigma,1), S_{\sigma,q})$, with $\sigma' = 1 - \sigma$ and $\sigma \in \{0,1\}$, we note that there are only 10 distinct configurations of the neighborhood. Let us take the example $\underline{\sigma}^0 = \{1,1,1,1,1\}$. A transition $1 \rightarrow 0$ of the center cell would lead to the extinction of 4 doublets $(\sigma, \sigma_j) = (1,1)$. On the other hand, the transition rate of the center cell is ε as known from eq. (12). This would result in $w((0,1)|(1,1), S_{1,4}) \propto 4\varepsilon$. However, for a lattice of size N the number of doublets is $2N$, whereas there are exactly N neighborhoods $\underline{\sigma}^0$. Therefore, if we apply the transition rates of the single cells (eq. (12)) to the transition of the doublets, their rates have to be scaled by 2. Similarly, if we take the example $\underline{\sigma}^0 = \{0,1,1,1,0\}$, a transition of the center cell $0 \rightarrow 1$ would occur at the rate $1 - \alpha_2$ and would create 3 new doublets. Applying the scaling factor of 2, we verify that $w((1,1)|(0,1), S_{0,1}) = 3/2 (1 - \alpha_2)$. This way we can determine the other possible transition rates:

$$\begin{aligned} w((0,1)|(1,1), S_{1,4}) &= 2\varepsilon \\ w((0,1)|(1,1), S_{1,3}) &= \frac{3}{2}\alpha_1 \\ w((0,1)|(1,1), S_{1,2}) &= \alpha_2 \\ w((0,1)|(1,1), S_{1,1}) &= \frac{1}{2}(1 - \alpha_2) \\ w((0,1)|(1,1), S_{1,0}) &= 0 \\ w((1,1)|(0,1), S_{0,4}) &= 0 \\ w((1,1)|(0,1), S_{0,3}) &= \frac{1}{2}\alpha_1 \\ w((1,1)|(0,1), S_{0,2}) &= \alpha_2 \\ w((1,1)|(0,1), S_{0,1}) &= \frac{3}{2}(1 - \alpha_2) \\ w((1,1)|(0,1), S_{0,0}) &= 2(1 - \alpha_1) \end{aligned} \quad (\text{A5})$$

Note that two of the transition rates are zero, because

the respective doublets (1,1) or (0,1) do not exist in the assumed neighborhood. Finally, we express the $\langle x_{\sigma,q} \rangle$ in eq. (A4) by the $\langle x_{\sigma,\underline{\sigma}'} \rangle$ of eq. (A3) and apply the pair approximation (eq. (31)) to the latter one. This way, we arrive at the dynamic equation for $\langle x_{1,1} \rangle$:

$$\begin{aligned} \frac{d \langle x_{1,1} \rangle}{dt} = & -2\varepsilon x c_{1|1}^4 \\ & + 2\alpha_1 \left[\frac{x}{(1-x)^3} (1-x + x c_{1|1})^3 (1 - c_{1|1}) \right. \\ & \quad \left. - 3x(1 - c_{1|1}) c_{1|1}^3 \right] \\ & + 6\alpha_2 \left[\frac{x^2}{(1-x)^3} (1-x + x c_{1|1})^2 (1 - c_{1|1})^2 c_{1|1}^2 \right. \\ & \quad \left. - x(1 - c_{1|1})^2 \right] \\ & + 2(1 - \alpha_1) \left[\frac{x^4}{(1-x)^3} (1 - c_{1|1})^4 \right. \\ & \quad \left. - x(1 - c_{1|1})^3 \right] \\ & + 2(1 - \alpha_2) \left[\frac{x^3}{(1-x)^3} 3(1 - 2x + x c_{1|1}) \times \right. \\ & \quad \left. \times (1 - c_{1|1})^3 - x(1 - c_{1|1})^3 c_{1|1} \right] \end{aligned} \quad (\text{A6})$$

The third equation (eq. (33)) for the correlation term $c_{1|1}$ can be obtained in explicit form by using eq. (A1) for $\langle x \rangle$ and eq. (A6) for $\langle x_{1,1} \rangle$:

$$\begin{aligned} \frac{dc_{1|1}}{dt} = & -\varepsilon \left(\frac{c_{1|1}}{x(1-x)^3} (1 - 2x + x c_{1|1})^4 + c_{1|1}^5 - 2c_{1|1}^4 \right) \\ & + \alpha_1 (1 - c_{1|1}) \left[c_{1|1}^3 (4c_{1|1} - 6) \right. \\ & \quad \left. - 2 \frac{1}{(1-x)^3} (1-x + x c_{1|1})^3 (2c_{1|1} - 1) \right] \\ & + 6\alpha_2 (1 - c_{1|1})^3 \left[\frac{x}{(1-x)^3} (1-x + x c_{1|1})^2 - c_{1|1} \right] \\ & + (1 - \alpha_1) (1 - c_{1|1})^4 \left[\frac{x^3}{(1-x)^3} (2 - c_{1|1}) + c_{1|1} \right] \\ & + (1 - \alpha_2) (1 - c_{1|1})^3 \left[2c_{1|1} (2c_{1|1} - 1) \right. \\ & \quad \left. + \frac{x^2}{(1-x)^3} (1 - 2x + x c_{1|1}) (6 - 4c_{1|1}) \right] \end{aligned} \quad (\text{A7})$$

-
- [1] J. Antonovics and P. Kareiva, *Philos. Trans. R. Soc. London B* **319**, 601 (1988).
 - [2] J. Molofsky, R. Durrett, J. Dushoff, D. Griffeth, and S. Levin, *Theoretical Population Biology* **55**, 270 (1999).
 - [3] F. J. Rohlf and G. D. Schnell, *American Naturalist* **105**(295-324) (1971).
 - [4] M. Kimura and G. H. Weiss, *Genetics* **49**, 313 (1964).
 - [5] P. S. Albin, *The Analysis of Complex Socioeconomic Systems* (Lexington Books, London, 1975).
 - [6] T. Schelling, *American Economic Review* **59**, 488 (1969).
 - [7] W. Weidlich, *J. Mathematical Sociology* **18**, 267 (1994).
 - [8] F. Schweitzer and J. Holyst, *European Physical Journal B* **15**(4), 723 (2000).
 - [9] A. Nowak, M. Kus, J. Urbaniak, and T. Zarycki, *Physica A* **287**(3-4), 613 (2000).
 - [10] J. Holyst, K. Kacperski, and F. Schweitzer, *Physica A* **285**, 199 (2000).
 - [11] P. L. Krapivsky and S. Redner, *Physical Review Letters* **90**(23), 238701 (2003).
 - [12] R. N. Costa Filho, M. P. Almeida, J. S. Andrade, and J. E. Moreira, *Physical Review E* **60**(1), 1067 (1999).
 - [13] A. T. Bernardes, D. Stauffer, and J. Kertesz, *European Physical Journal B* **25**(1), 123 (2002).
 - [14] N. A. Oomes, in *New Constructions in cellular automata*, edited by D. Griffeth and C. Moore (Oxford University Press, 2002), pp. 207–230.
 - [15] J. T. Cox and D. Griffeth, *Annals of Probability* **14**(2), 347 (1986).
 - [16] R. A. Holley and T. M. Liggett, *Annals of Probability* **3**, 643 (1975).
 - [17] T. M. Liggett, *Annals of Probability* **22**(2), 764 (1994).
 - [18] T. M. Liggett, *Stochastic Interacting Systems*, vol. 342 of *Grundlehren der mathematischen Wissenschaften* (Springer, Berlin, 1999).
 - [19] K. Sznajd-Weron and J. Sznajd, *International Journal of Modern Physics C* **11**(6), 1157 (2000).
 - [20] D. Stauffer, A. O. Sousa, and S. M. de Oliveira, *International Journal of Modern Physics C* **11**(6), 1239 (2000).
 - [21] D. Stauffer, *Journal of Artificial Societies and Social Simulation* **5**(1) (2001), URL <http://www.soc.surrey.ac.uk/JASSS/5/1/4.html>.
 - [22] L. Behera and F. Schweitzer, *International Journal of Modern Physics C* ??(??), ?? (2003), (in press), URL cond-mat/0306576.
 - [23] K. Lindgren and M. G. Nordahl, *Physica D* **75**, 292 (1994).
 - [24] G. Szabó and T. Csaba, *Physical Review E* **58**(1), 69 (1998).
 - [25] G. Szabó, T. Antal, P. Szabó, and M. Droz, *Physical Review E* **62**, 1095 (2000).
 - [26] F. Schweitzer, L. Behera, and H. Mühlenbein, *Advances in Complex Systems* **5**(2), 269 (2002).
 - [27] L. Behera, F. Schweitzer, and H. Mühlenbein, *Physica A* ??(??), ?? (2003), submitted.
 - [28] H. Mühlenbein and R. Höns, *Advances in Complex Systems* **5**(2), 301 (2002).
 - [29] D. Spiegelhalter and S. Lauritzen, *Networks* **20**, 579 (1990).
 - [30] J. Pearl, *Probabilistic Reasoning in Intelligent Systems: Networks of Plausible Inference* (Morgan Kaufman, San Mateo, 1988).
 - [31] R. Jiroušek and S. Preučil, *Computational Statistics & Data Analysis* **19**, 177 (1995).
 - [32] F. Jensen and F. Jensen, in *Proceedings of the Tenth Conference on Uncertainty in Artificial Intelligence*, edited by R. Mantaras and D. Poole (Morgan Kaufmann, San Francisco, 1994), pp. 360–366.
 - [33] T. M. H. Mühlenbein and A. Ochoa, *Journal of Heuristics* **5**(2), 213 (1999).
 - [34] F. Schweitzer, *Brownian Agents and Active Particles. Collective Dynamics in the Natural and Social Sciences*, Springer Series in Synergetics (Springer, Berlin, 2003).